



UPTAKE OF Co(II), Pb(II) AND Ni(II) IONS BY *Annona senegalensis* STEM BARK BIOCHAR FROM AQUEOUS SOLUTION: OPTIMIZATION, KINETIC AND THERMODYNAMIC STUDIES

*^{1,2}Aminu Omale, ^{1,2}Nwachukwu R. Ekere, ³Jamila A. Omale, ¹Janefrances N. Ihedioha and ²Samuel A. Egu

¹Department of Pure & Industrial Chemistry, University of Nigeria, Nsukka, Nigeria.

²Department of Pure & Industrial Chemistry, Kogi State University, Anyigba, Nigeria.

³Genomics and Molecular Biotechnology Research Laboratory, Department of Biochemistry, Kogi State University, Anyigba, Nigeria.

*Corresponding authors' email: omale.a@ksu.edu.ng Phone: +2348057289183

ABSTRACT

The concern for heavy metal pollution in the environment is especially so since they are non-biodegradable. The use of agro materials in the removal of these heavy metal pollutants has been recognized as a low-cost alternative to the costly conventional remediation techniques. The equilibrium sorption of the chemically activated *Annona senegalensis* stem bark was investigated. Using standard techniques, the physicochemical properties of activated carbon (MAASC) were ascertained. By using a simultaneous batch adsorption approach, the adsorption of Co²⁺, Pb²⁺, and Ni²⁺ onto MAASC was examined as a function of pH, solution temperature, initial metal ion concentration, agitation time, adsorbent dose, particle size, and carbonization temperature. The equilibrium sorption data generated were fitted into Langmuir, Freundlich, Temkin and Dubinin-Radushkevich isotherm models as well as pseudo first-order, pseudo-second-order and intraparticle diffusion kinetic models. From the obtained results, it was discovered that the Langmuir isotherm provided the best match conformation of all the models, except for Pb²⁺, which was best for Freundlich with an R² of 0.95. Physisorption was shown to be the mechanism by Dubinin-Radushkevich. For Co²⁺, Pb²⁺, and Ni²⁺, respectively, the pseudo second-order kinetic model had R² values of 0.997, 0.999, and 0.999 that best matched the data. Both intraparticle diffusion and the boundary layer effect also contributed to regulating the rates of the adsorption process. The study's thermodynamic results showed that H⁰ for Co²⁺, Pb²⁺, and Ni²⁺ were 27.51, 19.70, and 13.37 KJ/mol, respectively. These values are all positive and suggest an endothermic reaction, supporting the physisorption mechanism.

Keywords: Adsorption, Environmental pollution, Wastewater, Isotherm, Heavy metals

INTRODUCTION

Heavy metal pollution in the aquatic environments have become sources of great concern because these heavy metals are usually present in wastewater which is released to the environment from various industrial complexes. This concern is genuine and especially so since the heavy metals are non-biodegradable and accumulate in living systems resulting in various diseases. This fear has been heightened in recent times due to advancements in technology (Ameh et al., 2016).

The removal of contaminants in industrial wastewater is an important issue in countries with limited economic resources for the removal of pollutants generated by incipient industrial activity. Agro-waste products are receiving increased attention as raw materials in water and wastewater pollution control because of their cheap capital cost, availability and more importantly, they are environmentally friendly. Therefore, they present an important alternative to conventional methodologies (Adeyinka et al., 2019).

Chemical precipitation, electrolytic extraction, ion exchange, and other conventional methods are used to remove metals from aqueous solutions. Due to their high cost, inability to remove metals at low concentrations, and low pH tolerance, these procedures are no longer preferred. It is known that nickel poisoning prevents the development of the kidney, amylase enzymes, insulin, and spermatogenesis (Ameh et al., 2016).

Since the beginning of medicine, natural goods, particularly those made from plants, have been used to support human health. Plant phytochemicals have played a key role in pharmacological discoveries throughout the past century. Significant scientific interest in these chemicals' biological activities has been sparked by the significance of plant's

active components in both agriculture and medicine (Moghadamtousi et al., 2015; Okhale et al., 2016). Research in both the basic and practical sciences has conclusively shown that particular plant species have the genetic ability to remove, degrade, metabolize, or immobilize a variety of pollutants. Among them is *Annona senegalensis* Persoon, a plant (*Annonaceae*). The purpose of this study is to assess the efficacy of *Annona senegalensis* stem bark biochar as a low-tech, environmentally friendly green adsorbent and more importantly to document its kinetics and thermodynamics of adsorption. It has never been documented in the literature.

MATERIALS AND METHODS

The chemicals used are commercially available Analar grade reagents and require no further purification. The distilled and deionized water used were fully characterized. *Annona senegalensis* is a species of flowering plant in the custard apple family, *Annonaceae*. It is also known as the African custard apple, wild custard apple, wild soursop, sunkungo (Mandinka language), dorgot (Wolof language), and ukpokpo (Igala language). The specific epithet *senegalensis*, which refers to the nation where the original specimen was found, translates to "of Senegal." The fruits of *A. senegalensis*, a traditional food plant in Africa, may enhance nutrition, increase food security, promote rural development, and aid in sustainable land management.

Annona senegalensis stem bark was collected from the Muslim High School farm in Anyigba, Kogi State and stored in polyethylene bag before taking to the laboratory facility of the Department of Pure and Industrial Chemistry, Kogi State University, Anyigba. Sample pre-treatment was carried out in the laboratory. The plant was identified by a staff of the Plant

Science and Technology Department of Kogi State University, Anyigba. The stem bark was thoroughly washed with water and then pulverized before washing extensively with deionized water to remove any adhering dirt. The sample was sundried for two weeks and oven-dried at 105°C for 6h and thereafter, ground into powder using the grinding mill. The dried stem bark powder was sieved into different particle sizes (0.154, 0.180, 0.280, 0.450 and 0.900 mm) mesh sizes. The individually sieved fractions were stored in plastic containers for use as adsorbents.

Carbonization and activation

Carbonization of the adsorbent was carried out according to the method of Ekere et al., 2018. A 50 g mass each of dried *A. senegalensis* Stem Powder was carbonized in a muffle furnace at different temperature ranges (300°C, 350°C, 400°C, 450°C and 500°C) for 2 h each. At the end of 2 h, each of the samples was cooled in a desiccator for 3 h and then stored in air-tight bottle. The carbonized *A. senegalensis* Stem bark was activated via a chemical process. About 40 g were soaked in 250 mL of 25 % ZnCl₂ solution in five different 500 mL beakers for 24 h. After 24 hours, the mixture was filtered, and the residue was neutralized with diluted HCl before being cleaned with deionized water to a pH of 7.0. The samples were then dried at 105°C in a thermostatically controlled oven, and the product, which was given the name Modified Activated *Annona Senegalensis* Carbon, was then allowed to cool to room temperature (MAASC). The MAASC (stem-activated carbon from *A. senegalensis*) was kept in airtight bottles.

Physicochemical characterizations

Using a pH and conductivity meter that was already calibrated, the pH and conductivity were determined (Hanna instruments, model 0801). Using ASTM-recommended techniques, the percentages of moisture, ash, and volatile matter were measured. Using this technique, bulk density and porosity were determined according to Horsefall et al., 2011. The crystalline size and phases of the produced MAASC powders were determined using XRD spectroscopy. Before and after the batch adsorption investigations, the size, shape, and morphological characteristics of the adsorbents were examined using the SEM technique. The JCM-6000 NeoScope™ with connected energy dispersive X-ray spectroscopy was used to take all micrographs. Before and after metal adsorption investigations, the MAASC adsorbent's species and functional groups were identified using FT-IR spectroscopy. An Agilent Technologies Microlab FT-IR spectrometer with a Universal Single bounce Diamond ATR adapter was used to analyze the samples. Both FT-IR spectra were recorded in the range from 650 to 4000 cm⁻¹ in steps of 4 cm⁻¹.

Adsorption procedure

Unless otherwise noted, all stock solutions were made using analytical-grade reagents. Each day, new working standards were created by properly diluting the stock solutions. The effects of pH (2, 4, 6, 8 and 10) and adsorbent dosage (0.5, 1.0, 1.5, 2.0, and 2.5g), agitation time (5, 10, 20, 30, 40, 60, 80, and 100 minutes), initial adsorbate solution (5, 10, 15, 20 and 25 mg/L), and solution temperature were examined in batch mode adsorption studies for individual metal ions (303K, 308, 313, 318 and 323K). Additionally, the effects of particle sizes (0.154, 0.180, 0.280, 0.450, and 0.900 mm) and carbonization temperatures (300, 350, 400, 450, and 500°C) were investigated by placing 50 mL of metal ion solution (20 mg/L) in a test tube. The solutions (50mL) containing adsorbate and adsorbent were taken in 250mL capacity

conical flasks and agitated at 150 rpm on a mechanical shaker (Bellco Biotechnology Orbital Shaker, Vineland NJ, USA.) for 60minutes. The suspension was then filtered, and the supernatant was determined using Buck Scientific 210 FAAS. The amount of adsorption at equilibrium, q_e (mg g⁻¹), was calculated by:

$$q_e = \frac{(C_o - C_e)V}{W} \text{-----} \tag{1}$$

where C_o and C_e (mg l⁻¹) are the liquid-phase concentrations of metal ions at initial and equilibrium, respectively. V is the volume of the solution (l), and W is the mass of dry adsorbent used (g). The equation below was used to calculate the proportion of metal ions removed from the aqueous solutions

$$\text{Percentage removal of metal ion, } E_a = \frac{C_o - C_e}{C_o} \times 100 \dots \tag{2}$$

Adsorption isotherm studies

The experimental data for the metal ion adsorption onto *A. senegalensis* was fitted to the four-parameter isotherm models. The Langmuir equation is given by

$$q_e = \frac{(q_{max}K_L C_e)}{1 + K_L C_e} \tag{3}$$

where C_e is equilibrium adsorbate concentration(mg g⁻¹). K_L is Langmuir constant related to adsorption capacity(mg g⁻¹), which means that a large surface area and pore volume will lead to a higher adsorption capacity and is related to the variation of the adsorbent's porosity and surface area. The following linear form can be used to represent the equation:

$$\frac{1}{q_e} = \frac{1}{q_{max}K_L} \left[\frac{1}{C_e} \right] + \frac{1}{q_{max}} \text{ -} \tag{4}$$

A plot of 1/q_e against 1/C_e gives a straight line with a slope of (1/q_{max}K_L) and an intercept of 1/q_{max}.

Or

$$\frac{C_e}{q_e} = \frac{C_e}{q_{max}} + \frac{1}{q_{max}b}$$

A plot of C_e/q_e against C_e also gives a straight line.

The Freundlich model is an empirical equation just like the Langmuir model. It is used to estimate the adsorption intensity of sorbent towards the adsorbate. It is given by

$$q_e = K_F C_e^{(1/n)} \text{-----} \tag{5}$$

where K_F is adsorption capacity (L/mg) and 1/n is adsorption intensity; it also indicates the relative distribution of the energy and the heterogeneity of the adsorbate sites. Linearizing equation (5) we have

$$\log q_e = \log K_F + \frac{1}{n} \log C_e \text{ --} \tag{6}$$

a plot of log q_e against log C_e gives a straight line with (1/n) as the slope and log K_F as the intercept. The corresponding constants and coefficient of correlation (R²) associated with each linearized model at 25°C for the metal ions would be calculated.

The Temkin equation is

$$q_e = \frac{RT \ln A_T}{bT} + \frac{RT \ln C_e}{bT} \text{ or } q_e = B \ln A + B \ln C_e \tag{7}$$

where B = RT/b_T relating to the heat of adsorption, R is the universal gas constant, b_T is the adsorption potential of the adsorbent (J/mol) and A is the equilibrium binding constant (L/mg). The parameters for the Temkin model are obtained from the plot of q_e against lnC_e.

The Dubinin-Radushkevich (D-R) equation is represented in a linear form by

$$\ln q_e = \ln Q_0 - K_{DR} \varepsilon^2 \quad (8)$$

where K_{DR} ($\text{mol}^2 \text{KJ}^{-2}$) is a constant related to the mean adsorption energy and ε is the Polanyi potential which is derived from the equation

$$\varepsilon = RT \ln \left(1 + \frac{1}{C_e} \right) \quad (9)$$

In q_e is plotted against ε^2 and the slope gives K_{DR} and the intercept yields the sorption capacity, Q_0 (mg/g).

Kinetic modelling studies

The rate of adsorption of trace components onto porous solid surfaces has been described using a variety of adsorption kinetic models. Pseudo-first order and pseudo-second-order kinetic models are the most often employed types. Based on the results of the experiments, the Langergren pseudo-first-order and pseudo-second-order kinetic models are used to examine the metal ion adsorption kinetics. The sorption rates would be calculated as follows,

$$\log(q_e - qt) = \log q_e - \frac{k_1 t}{2.303} \quad (10)$$

Where q_e is the amount of metal ions adsorbed at equilibrium (mg/g); q_t is amount of metal ions adsorbed at time, t (mg/g); k_1 is Pseudo-first-order rate constant (g/mg/min) and t is the time (min). A graph of $\log(q_e - qt)$ versus t is plotted where the pseudo-first-order rate constant, k_1 and q_e are estimated from the slope and the intercept.

The linear form of second-order kinetic equation is

$$\frac{t}{qt} = \frac{1}{K_2 q_e^2} + \frac{1}{q_e} t \quad (11)$$

where q_e is the amount of metal ions adsorbed at equilibrium (mg/g); q_t is the amount of metal ions adsorbed at time t , (mg/g), k_2 is Pseudo-second-order rate constant (g/mg/min) and t is time (min)

Just like in the first order, a graph is drawn between t/qt versus t . The pseudo-second-order rate constant, K_2 and q_e are obtained from the intercept and slope respectively.

The initial rate of intra-particle diffusion is estimated using the following equation in accordance with the intra particle model proposed by Weber and Morris (1963).

$$qt = K_{diff} t^{0.5} + C \quad (12)$$

where qt is the amount of adsorbate deposited on the adsorbent (mg/g), and K_{diff} ($\text{mg/g min}^{0.5}$) gives the intra -

particle diffusion rate constant, t is the time of contact between adsorbate and adsorbent (min) and C is the intercept. From concentration versus time data, qt is obtained for different agitation times. A graph is drawn between qt and $t^{0.5}$. The standard free energy (ΔG°), standard enthalpy change (ΔH°) and standard entropy change (ΔS°) were evaluated to assess the feasibility of the adsorption process. ΔG° is given by the equation:

$$\Delta G^\circ = \Delta H^\circ - T \Delta S^\circ \quad (13)$$

The ΔG° is standard Gibbs free energy related to the thermodynamic equilibrium constant (K_c) thus:

$$\Delta G^\circ = RT \ln K_c \quad (14)$$

Where,

T = temperature (K); R = ideal gas constant (8.314 J/mol K) and K_c is defined by the equation:

$$K_c = \frac{C_a}{C_e} \quad (15)$$

where C_a and C_e are the metal ion concentration adsorbed from solution at equilibrium (mg/L) and the equilibrium metal ion concentration in the solution (mg/L) respectively. The Gibb's free energy (ΔG°), the enthalpy change (ΔH°) and the entropy change (ΔS°) have a relationship at a constant temperature by the Van't Hoff equation as shown below:

$$\ln K_c = \left(-\frac{\Delta G^\circ}{RT} \right) = -\frac{\Delta H^\circ}{RT} + \frac{\Delta S^\circ}{R} \quad (16)$$

The values of enthalpy change (ΔH°) and the entropy change (ΔS°) were estimated from the slope and intercept of the plot of $\ln K_c$ versus $1/T$. This equation is used to study the variation of the thermodynamic equilibrium constant with temperature.

RESULTS AND DISCUSSION

Table 1 displays the results of the physicochemical analyses of *Annona senegalensis* stem bark. Volatile matter, bulk density, porosity, pH, moisture and ash levels, and electrical conductivity are only a few of the characteristics examined.

Table 1: Physicochemical parameters of *Annona senegalensis* stem bark

Parameters	Value
pH	6.3 ± 0.61
Moisture content (%)	11.73 ± 0.2
Ash content (%)	7.21 ± 0.02
Volatile matter (%)	18.2 ± 1.00
Bulk density (g/cm ³)	0.18 ± 0.07
Porosity	0.995 ± 0.08
Electrical conductivity (μS/cm)	180.00 ± 2.09
Fixed carbon (%)	62.85 ± 0.94

All parameters were determined in triplicates and values are Mean±SD.

Microscopic and Spectroscopic characterization

Fig. 1a displays the raw adsorbent's XRD pattern. In Fig. 1a, some distinctive peaks are seen at 2θ values between 15θ and 25θ and 30θ and 40θ . The carbonized adsorbent's peak pattern (Fig. 1b) has a somewhat different shape. The peaks in 1a are broad, but the peaks in 1b are often pointy and sharp. The amorphous nature of the adsorbent in its raw powder form

in Fig. 1a explains why the activated product in 1b is crystalline. Sharp peaks with unique shapes were seen at positions 27θ , 29θ , 33θ , 36θ , 38θ , 39θ , 43θ , 48θ , 49θ , 58θ , 59θ , 65θ , and 66θ . The XRD peaks show nanoscale particles and are near the carbon allotrope of graphite. A non-destructive method that exposes a compound's crystalline structure is XRD (Syed et al., 2016).

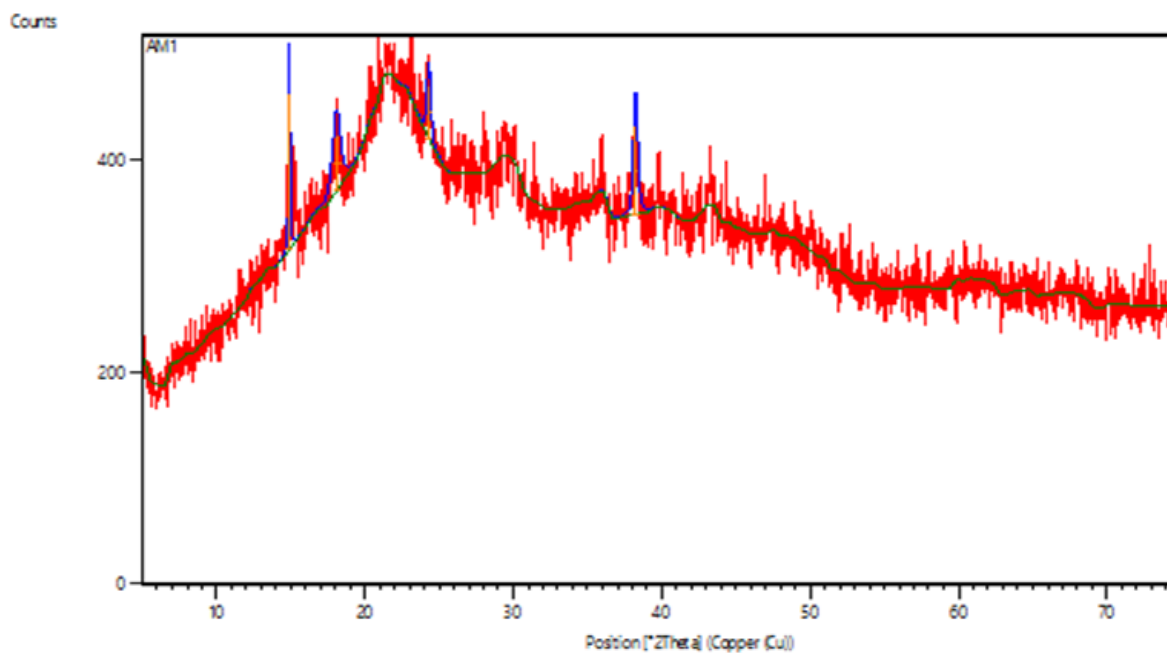


Figure 1a: XRD spectrum of raw *Annona senegalensis* powder.

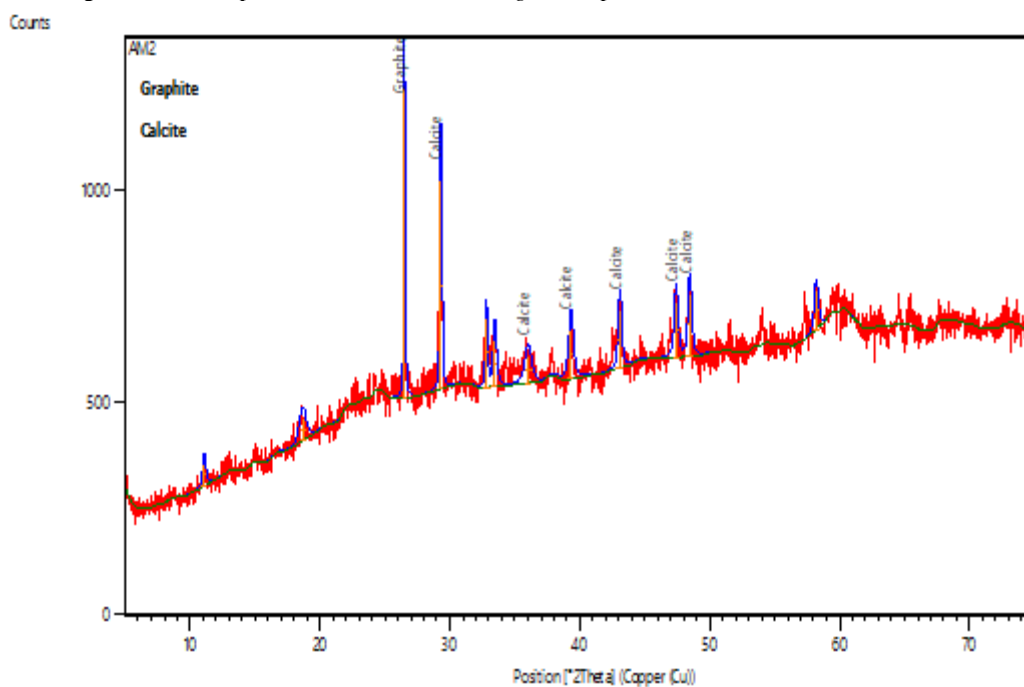


Figure 1b: XRD spectrum of metal-loaded modified *Annona senegalensis* activated carbon (MAASC)

The SEM analysis findings for raw and chemically activated MAASC, respectively, are shown in Figures 2a and b. The outcome demonstrated the presence of sheet particles that appear to be scattered hexagons (Fig 2a). The activated

adsorbent's morphology (Fig. 2b) was noticeably different since it was found to be rather rough and uneven in shape, but it also had pores with white sheets where heavy metal binding is presumed to have occurred.

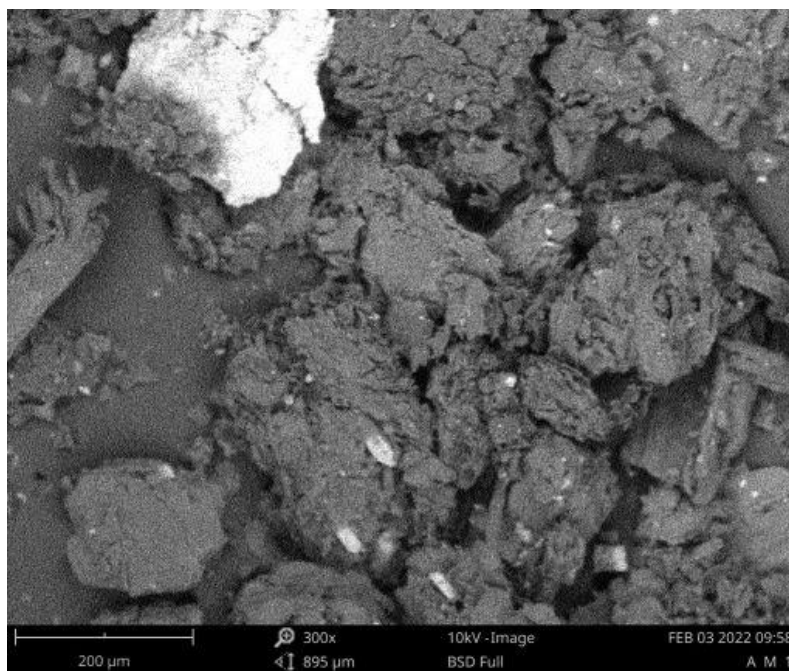


Figure 2a: SEM images of raw *Annona senegalensis* powder

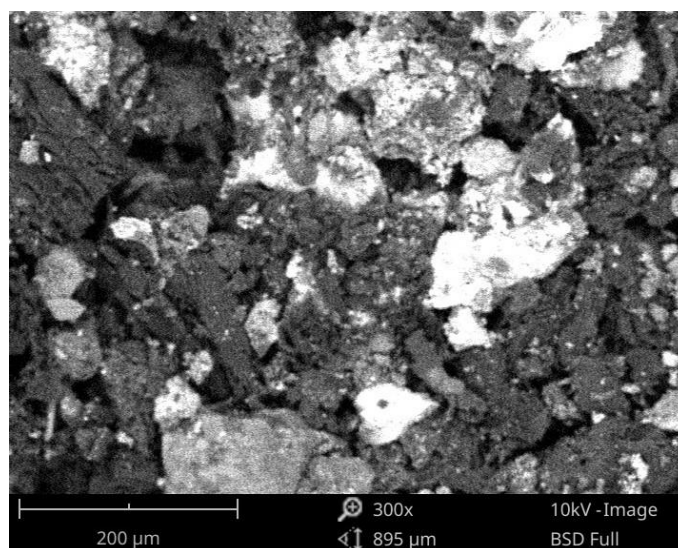


Figure 2b: SEM images of metal-loaded modified activated *Annona senegalensis* carbon (MAASC)

The presence of several of the adsorbent's peaks was confirmed by the FTIR spectra (Fig 3a and b). The raw adsorbent's spectrum before activation is shown in Fig. 3a. O-H stretching group is indicated by the large peak found at 3339.7cm^{-1} in the raw biosorbent. The other notable peaks at wavenumbers (cm^{-1}) 2918.5 - 2847.7 are associated with the C-H stretching vibrations of aliphatic groups, 1736.9 with the C=O vibrations of carbonyl groups, 1599.0 with the C-O stretching vibrations of carboxyl groups, and 1032.5 and

875.9 with the S-O stretching and S=O bands, respectively. The main peaks changed to 3488.8, 1446.2, 1066.0, and 700.7cm^{-1} after chemical activation, metal ion adsorption, and functionalization (3b). The best intensities for these peaks ranged from 98.47 to 98.67%. The fact that some of the peaks present in the raw biosorbent's spectra disappeared after activation indicated that the raw adsorbent had changed as a result of chemical treatment.

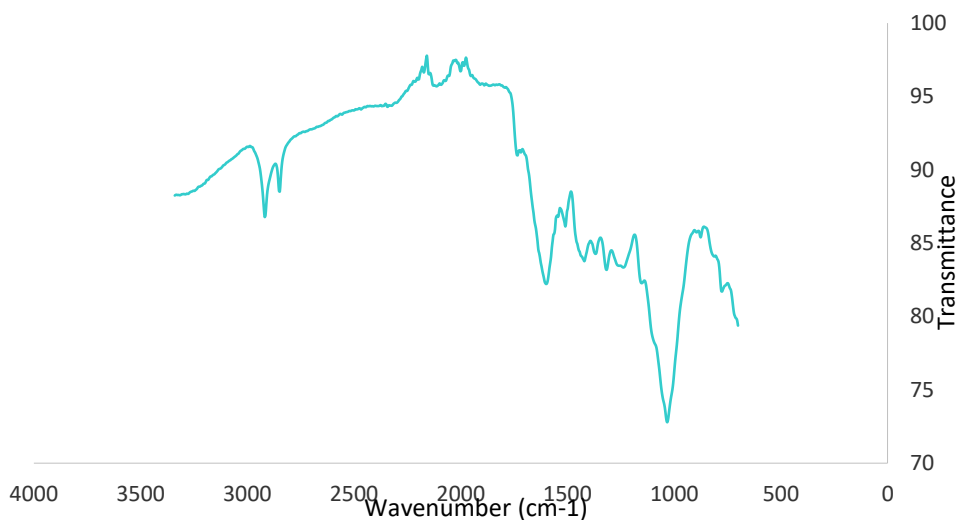


Figure 3a: FTIR spectrum of raw *Annona senegalensis* powder

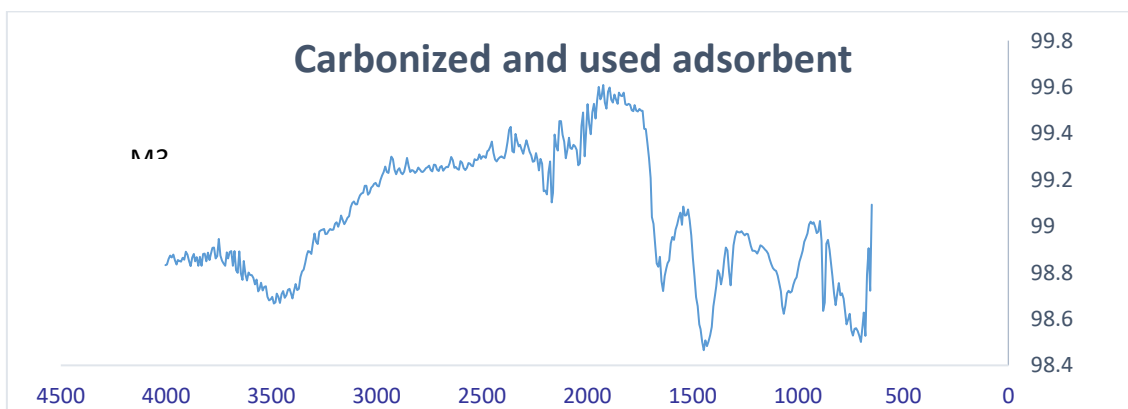


Figure 3b: FTIR spectrum of heavy metal loaded modified activated *Annona senegalensis* carbon (MAASC)

Effect of solution pH

Figure 4 depicts how solution pH affects the metal ion adsorption to MAASC. The findings show that uptake steadily rose to a maximum of 6 with a higher pH. At pH 4, Co²⁺, Pb²⁺, and Ni²⁺ maximal biosorption rates of 99.69, 88.20, and 85.93%, respectively, were noted. Due to the positively charged proton in the solution competing with the metal ions for the active site, adsorption was significantly

hindered at pH 2 to 5. Biosorption significantly increased as pH rose between 6 and 7, and some of the best outcomes were noted during this time. However, at higher pH levels (7–9), the biosorption of metal ions was again dramatically reduced, partially as a result of the production of the hydroxide anion, which reduced the concentrations of metal ions in the solution. This is consistent with studies conducted by Rahman and Sathasivan, (2015); and Xu et al., (2017).

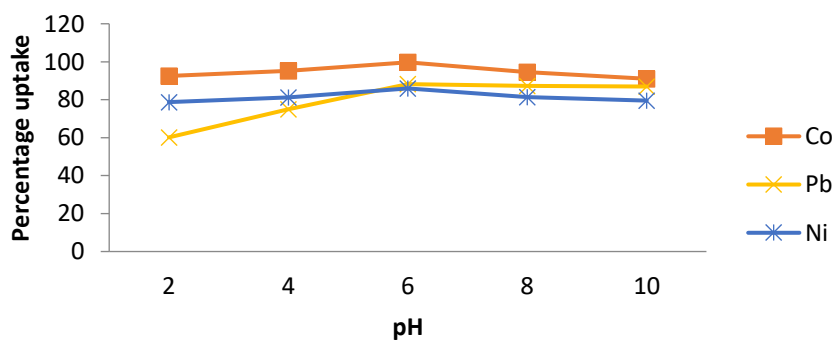


Figure 4: Effect of pH on heavy metal biosorption onto MAASC

Effect of adsorbent dose

Adsorbent dosage is crucial in a variety of ways because it establishes the extent of metal ion removal and, consequently, can be used to calculate the cost of remediation. Studies on the effects of different metal ions on MAASC were conducted at 30°C, pH 6, and variable doses between 0.5 and 2.5 g. The effects of the changes are shown in Fig. 5, where it can be

seen that an increase in MAASC mass resulted in a proportionate increase in the quantity of adsorption. At the maximum dosage of 2.5 g, the absorption of all the examined metals was at its highest. This is explained by the abundance of accessible adsorption sites. This presumption is consistent with previous works by Ameh et al., (2016) and Ekere et al., (2018).

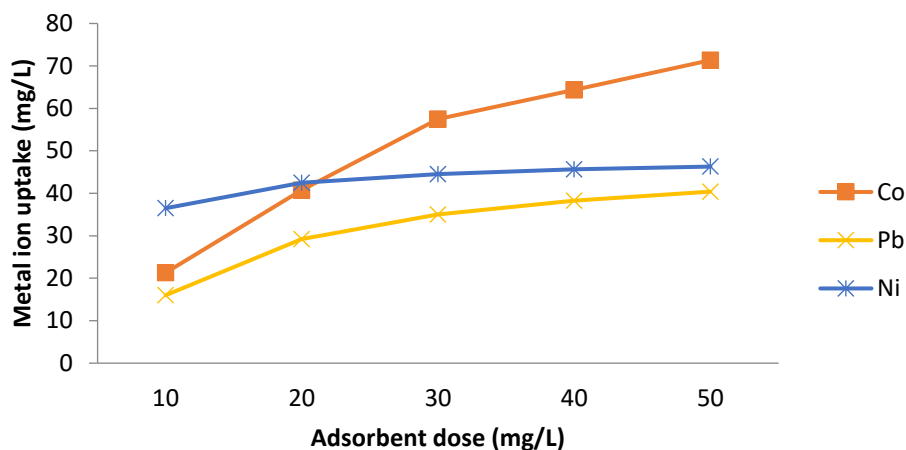


Figure 5: Effect of adsorbent dose on heavy metal biosorption onto MAASC

Effect of agitation time

Results from an investigation into how metal ion intake influences time are displayed in Fig. 6. The findings showed that, except for Pb²⁺, which reaches its maximum uptake after 40 minutes, the maximum uptake of 97.03, 59.40, and 86.76% for Co²⁺, Pb²⁺, and Ni²⁺ occurred at times over 80 minutes.

Additionally, the reduced uptake of the metal ions seen after about 80 minutes is indicative of the MAASC active site becoming saturated. However, several academic works asserted that the equilibrium biosorbent and contact time for biomass are reached around 90 minutes (Rahman and Sathasivan, 2015 and Ekere et al., 2018).

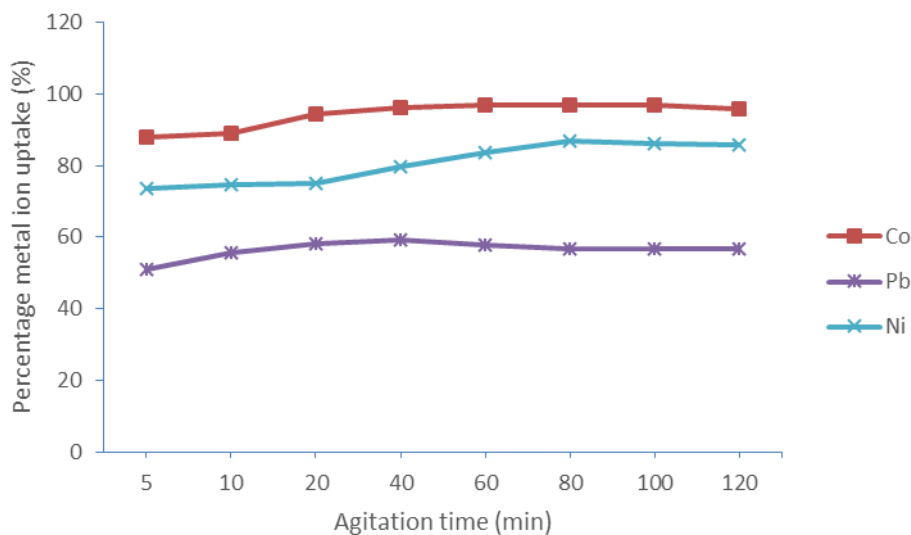


Figure 6: Effect of agitation time on heavy metal biosorption onto MAASC

Effect of initial metal ions concentration

Using different concentrations ranging from 5 to 25 mg/L, it was examined how the initial concentration of metal ions affected the effectiveness of their removal. According to the findings, the removal percentages of Co²⁺, Pb²⁺, and Ni²⁺ metal ions decreased steadily from 99.27 to 90.00%, 69.60 to

53.20%, and 92.39 to 81.92%, respectively. Since the initial concentration must have occupied all of the accessible active sites, this observation may be explained by the adsorbent's fixed nature. This outcome, as displayed in Fig. 7, is consistent with the studies of Yusuf et al., 2017.

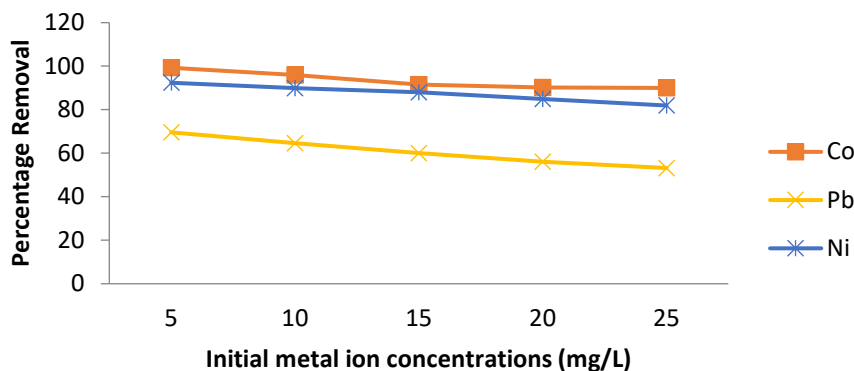


Figure 7: Effect of initial metal ion concentrations on heavy metal biosorption onto MAASC

Effect of solution temperature

Over a temperature range of 30 to 50°C, the impact of temperature on the removal of metal ions by MAASC was investigated. Fig. 8 displays the study's findings. All of the metal ions under study had already reached equilibrium at 45°C, with the exception of Co²⁺, which did so at 40°C. The observation revealed that Pb²⁺ and Ni²⁺ reached equilibrium at 45°C with 65.05 and 73.92%, respectively. At 40°C, however, Co²⁺ achieves equilibrium with a removal rate of

97.71% by biosorbent. This is a spontaneous occurrence, and it can be explained by the activation of MAASC biosorbent at higher temperatures, which led to the identification of more active sites for metal ion adsorption. Furthermore, the increased kinetic energy and mass transfer of metal ions may be the cause of reaching equilibrium before 50°C. This is consistent with work done by others (Oluwashola et al., 2019 and Umeh et al., 2021).

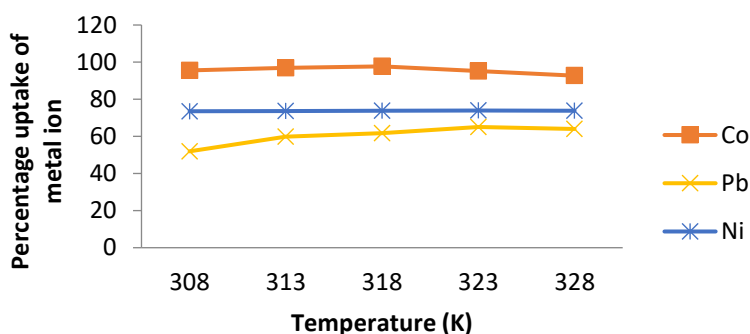


Figure 8: Effect of solution temperature on heavy metal biosorption onto MAASC

Effect of particle size

The MAASC was used to study the adsorption of metal ions with particle sizes of 0.154, 0.180, 0.280, 0.450, and 0.900mm. The results showed that as the particle size rose, the removal of metal ions reduced, as illustrated in Fig. 9. This suggests that the rate of uptake increases as the diameter of

the particle decreases. This might be explained by the fact that smaller particles have more surface area and, consequently, more adsorption-active sites. Larger particle size, on the other hand, leads to less adsorption. This might be because there aren't enough active sites for metal ion biosorption, which causes diffusion to mass transfer to be resistant.

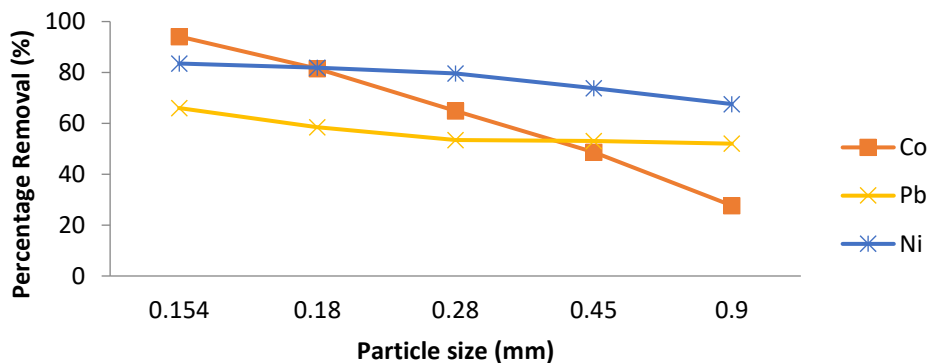


Figure 9: Effect of particle size on heavy metal biosorption onto MAASC

Effect of carbonization temperature

To test the impact of the carbonization temperature on the metal ions by MAASC biomass, the temperature ranging from 300 to 500°C were employed. Fig. 10 presents the evaluation's findings. The observed results showed that there was a commensurate rise in metal ion uptake when the temperature rose from 300°C to 350°C. The rate of metal uptake gradually increased when this occurred and started to decline beyond 400°C. This is due to material rearrangement brought on by

the action of increased heat, which results in the opening up of new active sites. However, as the temperature increased, adsorption rapidly attained saturation, which prevented absorption. This view is consistent with earlier research by Ekere et al., (2015) that found that at carbonization temperatures above 400°C, uptake substantially decreases while carbonization temperatures below 400°C increase the level of internal re-arrangement of materials by opening up more pores as heat is increased.

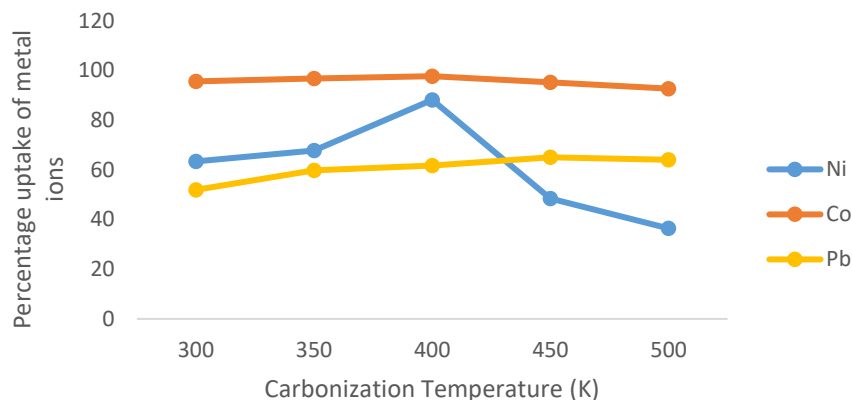


Figure 10: Effect of carbonization temperature on heavy metal biosorption onto MAASC

Adsorption isotherm studies

The link between the concentration of the adsorbate and its degree of adsorption onto the adsorbent surface, as well as details on the sorption mechanism, surface characteristics, and affinity of the adsorbent at a constant temperature, are all

revealed by the adsorption isotherm. The equilibrium results were analyzed using the Langmuir, Freundlich, Temkin, and Dubinin-Radushkevich isotherm models to maximize the MAASC's ability to adsorb Co(II), Pb(II), and Ni(II) ions from aqueous solution. Table 2 displays the analysis findings.

Table 2: Isotherm parameters for Co²⁺, Pb²⁺ and Ni²⁺ adsorption onto MAASC biosorbent

Model	Parameter	Metal ions		
		Co ²⁺	Pb ²⁺	Ni ²⁺
Langmuir	q_{max} (mg/g)	45.05	22.73	3.2248
	K_L (L/mg)	0.03154	0.04927	0.0082
	R_L	0.0016	0.092	0.0004
	R^2	0.9995	0.9171	0.9987
Freundlich	K_F	46.45	8.71	38.66
	n	25.58	1.6445	7.19
	R^2	0.8792	0.9531	0.993
Temkin	A_T (L/mg)	4.394	97.56	0.427
	b_T (KJ/mol)	563.853	25.395	5,802.2
	R^2	0.5703	0.936	0.9832
Dubini-Radushkevich	q_m (mg/g)	3.8584	3.7094	3.8589
	K_{DR} (mol ² /KJ ²)	3×10^{-6}	3×10^{-6}	1×10^{-7}
	R^2	0.4171	0.8969	0.9663
	E (KJ/mol)	0.408	0.408	2.236

The Langmuir isotherm model predicts that monolayer sorption will result in homogenous sites inside the adsorbent with no interaction between adsorbed species. K_L and R_L , respectively, provide the Langmuir equilibrium constant (L/mg) and the characteristics of the adsorption process. Adsorption is therefore regarded as irreversible if R_L equals

zero ($RL = 0$), favorable if RL is less than one ($RL < 1$), linear if RL is equal to one ($RL = 1$), and unfavorable if RL is higher than one ($RL > 1$). The RL of all the metal ions examined was 0.0016 for Co²⁺, 0.092 for Pb²⁺, and 0.0004 for Ni²⁺, all of which are below 1, indicating that they will all adsorb favorably.

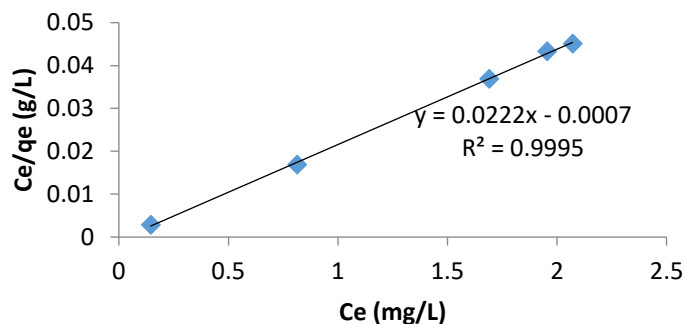


Figure 11: Langmuir isotherm model for Co²⁺ biosorption onto MAASC

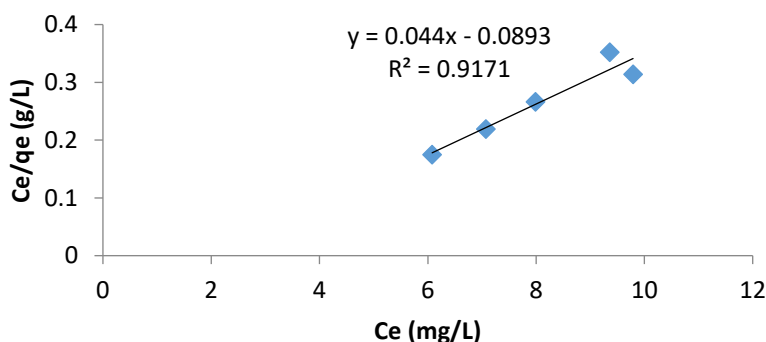


Figure 12: Langmuir isotherm model for Pb²⁺ biosorption onto MAASC

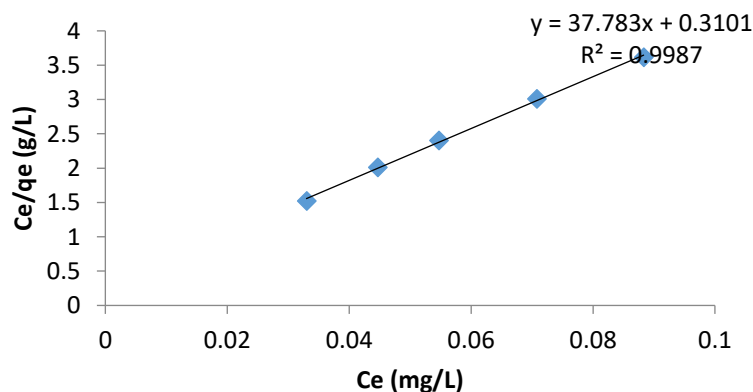


Figure 13: Langmuir isotherm model for Ni²⁺ biosorption onto MAASC

Due to its superior correlation coefficient (R^2), which is close to 1, the Langmuir isotherm provided a good conformation analysis of the equilibrium data when the correlation coefficients of all other isotherms used were compared. The Freundlich isotherm came next. The isotherm order for the metal ions' adsorption onto MAASC is as follows. Langmuir > Freundlich > Temkni > Dubinin-Radushkevich. When specific metal ions are taken into account, the Langmuir and Ni isotherms were shown to be the best fits for Co, with correlation coefficients (R^2) of roughly 1.00 and 1.00, respectively. With a correlation coefficient of roughly 0.95,

Freundlich's isotherm was, however, the one that fit Pb the best.

Adsorption kinetic studies

To analyze the obtained data and determine the rate and potential adsorption process, adsorption kinetic models were fitted. The findings are shown in Table 3 for the applied models, which include pseudo-first order, pseudo-second order, and intra-particle diffusion kinetic model equations. All of the kinetic model's equations were applied to the kinetic data.

Table 3: Biosorption kinetic models for the adsorption of metal ions onto MAASC biosorbent

Kinetic Models	Parameters	Metal ion		
		Co ²⁺	Pb ²⁺	Ni ²⁺
PFO	K_1 (min ⁻¹)	0.0106	0.0378	0.0233
	q_o (mg/g)	24.31	8.46	9.66
	R^2	0.885	0.997	0.984
PSO	K_2 (g/mg min)	0.00389	0.00807	0.00831
	q_e (mg/g)	39.22	30.86	38.91
	h (mg/g min)	5.983	7.685	12.581
IPD	$t_{1/2}$ (min)	0.167	0.130	0.0795
	R^2	0.997	1.000	1.000
	k_d (mg/g min ^{0.5})	3.0159	1.9026	1.8187
	C (mg/g)	13.54	15.35	23.79
	R^2	0.9423	0.9227	0.9882

According to the findings, pseudo-first-order kinetic model data is very helpful in characterizing the adsorption kinetics of the metal ions, particularly for Pb and Ni, which have R² values of 1.00 and 0.98, respectively. This excludes Co with a value of 0.89, hence it is insufficient to describe the kinetics

of metal ions adsorbing on MAASC. Similar observations regarding the biosorption kinetics of metal ions have been published in the literature (Rahman and Sathasivan, 2015; Arshadi et al., 2014).

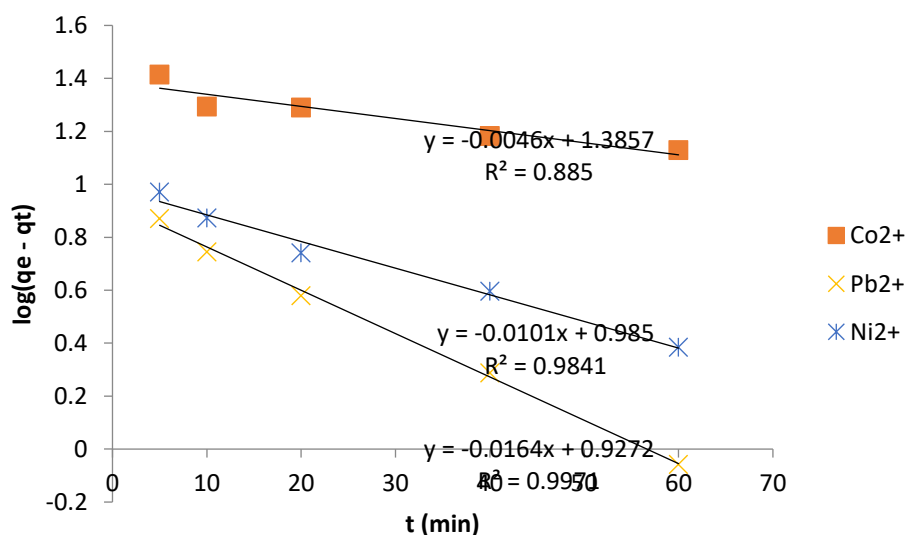


Figure 14: Pseudo-first-order kinetic model for metal ions biosorption onto MAASC

In Table 3 and Fig. 14, the solutions to the pseudo-second order kinetic model equations are also displayed. The pseudo-second-order equation demonstrated to be a superior model in explaining the experimental data, with the R² exhibiting superiority among the tested kinetic models with 1.00, 1.00, and 1.00 approximately for Co²⁺, Pb²⁺, and Ni²⁺ correspondingly. Given the initial uptake rate, h (2.090 to 12.581 mg/g min) in the first few minutes, where more than 75% of adsorption occurred, it was determined that the rate

constant, k_2 , ranged from 0.00064 to 0.00831g/mg min. This indicated that the spontaneity of the adsorption process was quick and favorable. Diffusion was therefore the process' rate-limiting stage. The duration of half-adsorption to take place, $t^{1/2}$, ranged from 0.07795 to 0.476 minutes showing high sorbate-sorbent affinity. This finding is consistent with other works published in the literature (Akpomie et al., 2015; Rahman and Sathasivan, (2015).

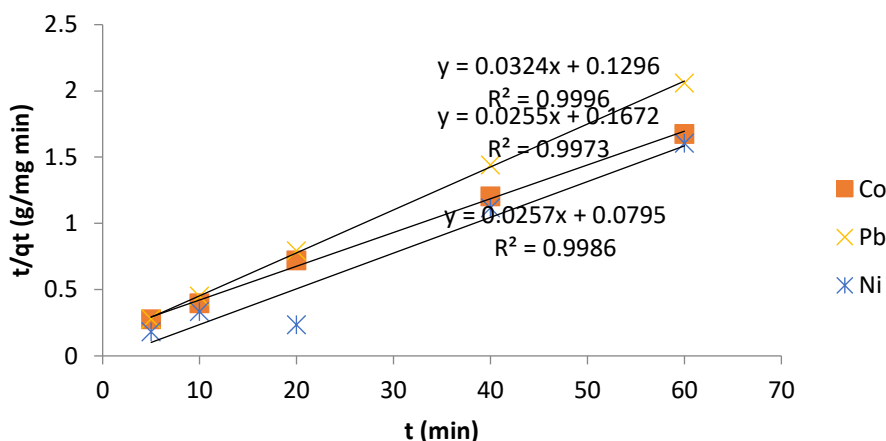


Figure 15: Pseudo second order kinetic model for metal ions biosorption onto MAASC

The Weber-Morris intra-particle diffusion model was also applied to the kinetic data; the results are shown in Table 3 and Fig. 15. Molecular diffusion is regarded as the most emblematic of all the transport processes out of all the physicochemical phenomena, including dimensional micelle creation, electro-kinetic interactions, and molecular diffusion. This might be because people frequently obstruct the gradient-oriented movement of migratory species. According to the results, *Kd* is the rate constant for intra-particle diffusion, and *C* is the intercept that veered away from the origin, suggesting that there are other rate-determining processes outside intra-particle diffusion. As a result, a boundary layer effect can be seen in the first curved part of

Fig. 16. Furthermore, the regression coefficients of 0.94 (Co^{2+}), 0.92 (Pb^{2+}), and 0.99 (Ni^{2+}) show that intra-particle diffusion plays a substantial role in the adsorption of the metal ions. The latter, linear-appearing segment of the curve illustrates this outcome. Although the R^2 of the intra-particle diffusion model was lower than that of the pseudo second order model, it was still higher than that of the pseudo first order model. This suggests that because the PSO kinetic model had the best regression coefficient, it provided a better treatment of the data. This result was anticipated, and additional researchers and the literature have confirmed this (Yusuf et al., 2017; Ekere et al., 2018 and Umeh et al., 2021).

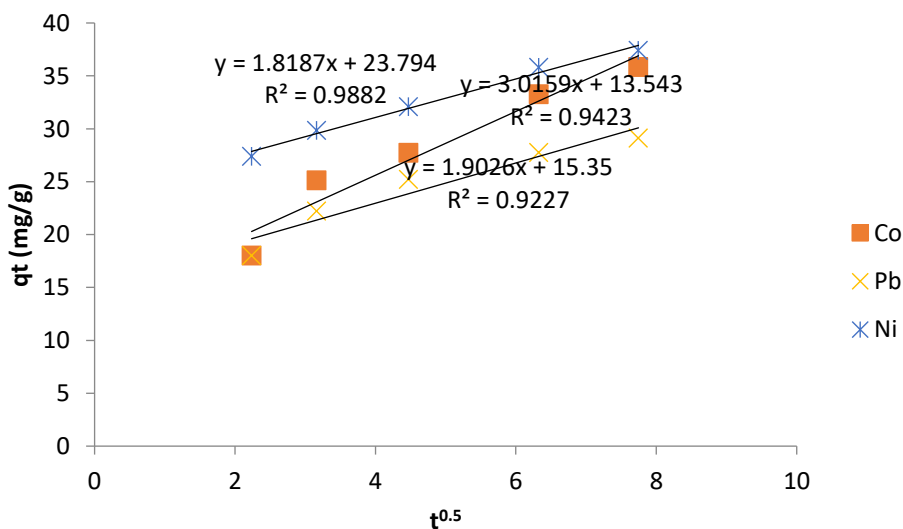


Figure 16: Intra-particle diffusion model for the metal ions biosorption onto MAASC

Adsorption thermodynamic studies

The values of the thermodynamic parameters for the metal ion biosorption onto MAASC are presented in Table 4. The linear

form of Van't Hoof plots of $\ln K_D$ versus $1/T$ is depicted in Fig 16.

Table 4: Thermodynamic parameters for the adsorption of metal ions onto MAASC biosorbent

Metal ion	ΔH (KJ/mol)	ΔS (KJ/molK)	ΔG (KJ/mol)					R^2
			308K	313K	318K	323K	328K	
Co^{2+}	27.5077	109.73	- 6.4799	- 6.9507	- 6.5851	- 7.5476	- 7.8684	0.9364
Pb^{2+}	19.7009	83.74	- 6.1657	- 6.6987	- 6.2658	- 7.0637	- 7.3037	0.9385
Ni^{2+}	13.3739	65.92	- 6.9208	- 7.3370	- 7.7469	- 7.7469	- 7.9860	0.9883

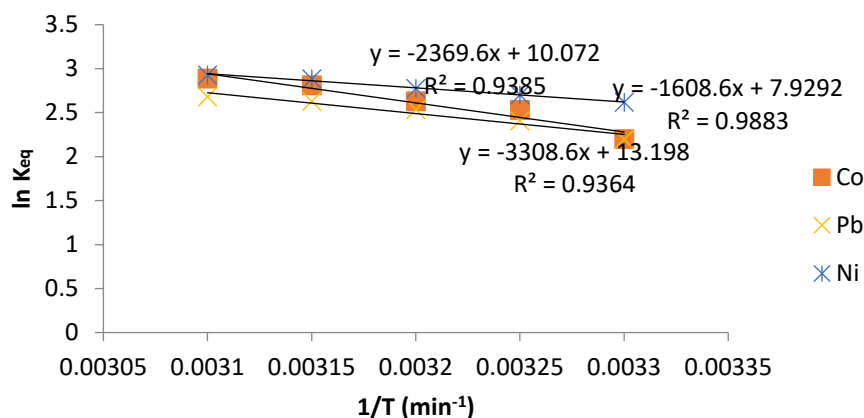


Figure 17: Thermodynamics Van't Hoff plot for metal ions biosorption onto MAASC

The negative values of ΔG° at the different temperatures show that the thermodynamic process of metal ion adsorption onto MAASC was both possible and spontaneous. Additionally, the increase in metal ion uptake with the rise in solution temperature from 308 to 328 K led to a positive change in enthalpy, which was a sign of an endothermic process. The magnitude of the enthalpy values is also indicative of the several kinds of biosorption mechanisms, including physisorption, chemisorption, and combinations of the two. For physical adsorption, ΔH° lies between 2.1 – 20.9 KJ/mol, for physical and chemical adsorption combined, ΔH° lies between 20.9 – 80.0 KJ/mol while for chemical adsorption, ΔH° lies between 80.0 – 200 KJ/mol. From our studies, Co^{2+} with ΔH° of 27.51 KJ/mol was adsorbed by a combination of both physical and chemical adsorption while Pb^{2+} and Ni^{2+} with ΔH° of 19.70 and 13.37 KJ/mol were clearly adsorbed by physisorption. The D-R isotherm model results, which showed that E values less than 8 KJ/mol are suggestive of physisorption, provide unambiguous proof for this claim. Additionally, a significant degree of disorderliness at the solid-liquid interface during the biosorption of metal ions onto MAASC is suggested by the thermodynamic parameter ΔS° , which is completely positive.

CONCLUSION

The process of heavy metal adsorption onto biomass derived from agriculture involves several different mechanisms. Adsorbent dose, beginning metal ion concentrations, solution pH, solution temperature, agitation or contact time, as well as initial concentrations of metal ions (Co, Pb, and Ni), were all significant factors in our investigation since they affected the rate and efficiency of the process. The outcomes demonstrated that maximum metal ion uptake was accomplished at contact times of 88 minutes, pH values of 6.0 and 30 degrees Celsius, metal ion concentrations of 5 mg/L, and adsorbent doses of 2.5 g. We looked at the adsorption of Co(II), Pb(II), and Ni(II) onto chemically activated MAASC. Since $RL < 1$ and the adsorption capacities of Co^{2+} , Pb^{2+} , and Ni^{2+} were 45.05 mg/g, 22.73 mg/g, and 3.22 mg/g at 30 °C, respectively, the equilibrium values fit the Langmuir isotherm model well.

All of the studied metal ions' kinetic data fit the PSO kinetic model better because it highlighted the rate-limiting step for sorbate-sorbent interactions and provided the best conformation for the sorption mechanism. IPD is another process that play a significant role in the adsorption process. The heavy metal adsorption onto MAASC was endothermic, practicable, and spontaneous, according to the

thermodynamic analysis. According to research using the Dubinin-Radushkevich isotherm model with fewer than 8 KJ/mol and thermodynamic results of the enthalpy change with less than 80 KJ/mol, the primary transport mechanism of the examined heavy metals is physisorption. As a result, this study demonstrated that activated carbon made from *A. senegalensis* can be used as an inexpensive, low-tech, ecologically friendly adsorbent for the removal of heavy metals from contaminated environment.

REFERENCES

- Adeyinka, G. C and Moodley, Brenda (2019). Effect of aqueous concentration of humic acid on the sorption of polychlorinated biphenyls onto particle grain sizes. *Journal of Soils and Sediments*, 19: 1543 – 1553.
- Akpomie, K. G., Dawodu, F. A and Adebawale, K. O (2015). Mechanism on the sorption of heavy metals from binary-solution by a low-cost montmorillonite and it's desorption potential. *Alex. Eng J*, 54(3): 757 – 767.
- Ameh, P. O., Ushe, M. U., James, F and Usman, U (2016). Removal of Ni (II) and Pb (II) from aqueous solution by adsorption onto *Vitex simplicifolia* nut activated carbon. *Journal of Applied Chemical Science International* 6(2): 85 – 90.
- Arshadi, M., Amiri, M. J and Mousavi, S (2014). Kinetic, equilibrium and thermodynamic investigations of Ni (II), Cd (II), Cu(II) and Co(II) adsorption on barley straw ash, *Water Resources and Industry*, 6: 1 – 17.
- Ekere, N. R., Agwogie, A. B and Ihedioha, J. N (2018). Removal of Pb(II), Cd(II), Cu(II) and Ni(II) ions from aqueous solution using *Pentaclethra macrophylla* stem activated carbon. *Pak. J. Anal. Environ. Chem*, 19(2): 195 – 204.
- Ekere, N. R., Agwogie, B. A and Ihedioha, J. N (2015). Studies of biosorption of Pb²⁺, Cd²⁺ and Cu²⁺ from aqueous solution using *Adansonia digitata* root powders. *Int. J. Phytoremediation*, 18: 329. <http://dx.doi.org/10.1080/15226514.2015.1058329>
- Horsfall, M; Ekpete, OA and Spiff, AI (2011). Fixed bed adsorption of chlorophenol on fluted pumpkin and commercial activated carbon. *Australian Journal of Basic and Applied Sciences*, 5(11): 1149 – 1155.

- Moghadamtousi S, Fadaeinasab M, Nikzad S, Mohan G, Ali H, Kadir H. (2015) *Annona muricata* (Annonaceae): A Review of Its Traditional Uses, Isolated Acetogenins and Biological Activities, *Int. J Mol Sci.*; **16**:15625 – 15658.
- Okhale, SE; Akpan, E; Fatokun, OT; Esievo, KB and Kunle, OF (2016). *Annona senegalensis* Persoon (Annonaceae): A review of its ethnomedicinal uses, biological activities and phytochemicals. *Journal of Pharmacognosy and Phytochemistry*, **5**(2): 211 – 219.
- Oluwasola, H. O., Asegbeloyin, J. N., Ochonogor, A. E., Ani, J. U., Ibeji, C. U and Oyeka, E. E (2019). Cadmium and lead adsorption capacities of Nigerian ultisol soil of tropics. *Oriental Journal of Chemistry*. **35**(3): 1004 – 1012.
- Rahman, M. S and Sathasivam, K. V (2015). Heavy metal adsorption onto *Kappaphycus sp* from aqueous solutions: The use of error functions for validation of isotherm and kinetics models. *BioMedical Research International*, <https://dx.doi.org/10.1155/2015/126298>.
- Syed, B, Prasad, N. M. N and Satish, S (2016). Endogenic mediated synthesis of gold nanoparticles bearing bacteriacidal activity. *Journal of microscopy and ultrastructure*. **4**: 162 – 166. <http://dx.doi.org/10.1016/j.jmau.2016.01.004>
- Umeh, T. C., Nduka, J. K and Akpomie, K. G (2021). Kinetics and isotherm modelling of Pb(II) and Cd(II) sequestration from polluted water onto ultisol obtained from Enugu, Nigeria. *Applied Water Science*, **11**: 65.
- Weber, W.J., and Morris, J.C., (1963). Kinetics of adsorption on carbon from solutions. *J. Sanit. Eng. Div.* **89**, 31 – 60.
- Xu, L., Zheng, X., Cui, H., Zhu, Z., Liang, J and Zhu, J (2017). Equilibrium, kinetic and thermodynamic studies on the adsorption of cadmium from aqueous solution by modified biomass ash. *Bioinorganic Chemistry and Applications* 2017.
- Yusuff, A. S., Olateju, I. I and Ekanem, S. E (2017). Equilibrium, kinetic and thermodynamic studies of the adsorption of heavy metals from aqueous solution by thermally treated quail eggshell. *Journal of Environmental Science and Technology*, **10**: 245 – 257.

